Multiplexed bio-imaging using cadmium telluride quantum dots synthesized by mathematically derived process parameters in a continuous flow active microreactor

S. Pandey [a,b], D. Mukherjee [c,e], P. Kshirsagar [d], C. Patra [b,c], D. Bodas [a,b,*]

[a] *Nanobioscience Group, Agharkar Research Institute, GG Agarkar Road, Pune, 411 004, India*
[b] *Savitribai Phule Pune University, Ganeshkhind Road, Pune, 411 007, India*
[c] *Developmental Biology Group, Agharkar Research Institute, GG Agarkar Road, Pune, 411 004, India*
[d] *Bioenergy Group, Agharkar Research Institute, GG Agarkar Road, Pune, 411 004, India*

A B S T R A C T

Quantum dots (QDs) are semiconductor nanocrystals with unique size-tunable emissions. To obtain a precise emission spectrum, monodispersity in size is imperative, which is achieved by controlling the reaction kinetics in a continuous flow of active microreactors. Further, a multivariate approach (dimensional analysis) is employed to impose stringent control on the reaction process resulting in monodispersed preparation of cadmium telluride (CdTe) quantum dots. Dimensional analysis knits multiple variables into a dimensionless mathematical form which not only predicts parameters precisely to obtain narrow size tunability but also guarantees reproducibility in synthesis. Analytical, structural, and optical characterization of the microreactor synthesized poly-dimethylsiloxane (PDMS) coated CdTe QDs reveal quantum efficient (61.5%), photostable (44%), and biocompatible nanocrystals of 5–15 nm. Further, PDMS-coated QDs (P-QDs) are conjugated with organelle-specific antibodies/biomarkers for *in-vitro* imaging in NIH 3T3 cells. Likewise, proliferating cell nuclear antigen (PCNA) and anti-myosin (MF20), cardiomyocytes antibodies are conjugated with P-QDs (red and green, respectively) to image the zebrafish's cardiac tissue. Antibodies tagged with quantum dots are imaged simultaneously using confocal microscopy. Thus, multiplexed bio-imaging of *in-vitro* and zebrafish tissue is demonstrated successfully. The results indicate the suitability of continuous flow active microreactor in conjunction with the mathematical prediction of process parameters to synthesize reproducibly monodispersed and quantum efficient QDs.

1. Introduction

Semiconductor nanocrystals, commonly termed as quantum dots (QDs), exhibit size-dependent fluorescence. Principally, QDs exhibit size-dependent emission due to the quantum confinement effect [1]. Moreover, they show unique properties such as high quantum efficiency, high fluorescence lifetime, narrow size-tunable emission spectra, biocompatibility, photothermal- and photochemical stability, which make them versatile in various applications [2–5]. Lately, QDs are used in multiplexed imaging as they exhibit size tunability with a narrow emission spectrum [6]. To enhance the application area of QDs, the synthesis of multiple colors with narrow emission will be desirable specifically for bio-imaging applications. Thus, control over the size of nanocrystals, or in other words, monodispersity during synthesis, is essential [7,8].

Recently, many researchers have attempted to obtain monodispersed preparation of QDs with desirable properties [9]. Stringent control over the synthesis process is imperative, which can be attained using microreactors [10–13]. Microreactors offer several advantages over conventional synthesis method such as: (1) low reagent consumption; (2) large surface area to volume ratio; (3) higher mixing efficiency; and (4) better heat transfer to reactions (specifically involving high temperature), to promote homogeneous nucleation and growth [14,15]. Thus, the use of a microreactor allows precise control of reaction parameters to yield monodispersed preparation. Many researchers have sought the

---

microreactor-based synthesis of quantum dots to achieve better control over reaction kinetics [3,16]. Richard et al. have demonstrated the narrow size distribution of quantum dots synthesized using a microreactor compared to batch synthesis [17]. Similarly, Wang et al. have reported controlled synthesis of quantum dots using microfluidics [18]. Table 1 showing the lower full width half maximum (FWHM) values of QDs synthesized via microreactor than a batch process.

Although a microreactor offers a better platform for controlled synthesis, the method involves tweaking individual variables. However, to reproducibly synthesize size-tunable QDs, a dimensionless mathematical equation for the accurate prediction of parameters was developed using the dimensional analysis method. Dimensional analysis is a multivariate approach that could mathematically illustrate the relationship between involved physical quantities derived from the experiments. Thus, obtained dimensionless mathematical equations can predict process parameters accurately to achieve superior control over nanoparticle synthesis [28–30].

Herein, we report a dimensional analysis approach to derive a dimensionless mathematical equation for predicting process parameters to synthesize size-tunable cadmium telluride quantum dots (CdTe QDs) using a microreactor. Further, to employ these nanocrystals for bio-imaging, polydimethylsiloxane (PDMS) was coated over CdTe QDs and confirmed using Fourier transform infrared (FT-IR) spectroscopy. Optical characterization of PDMS coated QDs (P-QDs) was carried out using photoluminescence (PL) spectroscopy, followed by the determination of quantum yield and photostability. Atomic force (AFM) and transmission electron microscopes (TEM) were used to determine the crystallite size, followed by the size distribution analysis.

The toxicity of P-QDs was assessed by 3-(4,5-dimethylthiazol-2-yl)-2,5-diphenyl tetrazolium bromide (MTT) assay. Additionally, Cd^{2+} ion leaching estimation was carried out by atomic absorption spectroscopy (AAS) to determine time-dependent release kinetics. Further, P-QDs were conjugated with actin and nucleus-specific antibodies for multiplexed imaging in NIH 3T3 cell line (the cell line, obtained from desegregated NIH Swiss mouse embryo fibroblasts; 3T3 stands for '3-day transfer, inoculum 3×10^{5} cells' and is derived from the original cell transfer and inoculation protocol). Furthermore, P-QDs were conjugated with cardiac tissue-specific markers anti-myosin heavy chain (MF20) and proliferating cell nuclear antigen (PCNA) of zebrafish to demonstrate tissue imaging.

2. Experimental section

2.1. Fabrication of microreactor and the synthesis of QDs and P-QDs

Microreactor was fabricated by soft lithography technique using polydimethylsiloxane (PDMS) [31] for carrying out the synthesis of QDs. Briefly, the prepolymer, and the curing agent were mixed in a 10:1 ratio and degassed for 30 min. A mold was constructed (Fig. 1a) by placing a copper wire of diameter 500 μm and length 50 mm. The wire was placed equidistant from the top and bottom of the mold. PDMS was then poured onto the assembly and cured for 3 h at 70 °C. After curing, the chip was demolded, and the copper wire was drawn out to obtain a circular microchannel (Fig. 1b). PDMS after curing (cross-linking) is plasticized and can withstand high temperatures

Table 1
Comparison of full width half maximum obtained from microreactor and batch synthesis of different types of quantum dots.

Types of QDs	Microreactor synthesis	Batch Synthesis	References
CdS	21–27 nm	–	[19]
CdSe	32 nm; 38 nm; 40–50 nm	125 nm	[12, 20–22]
CdTe; CdZnTe; CdTe/ZnS	40 nm	50 nm; 50–78 nm	[23–25]
ZnSe/Zn; Mn:ZnSe/Cu:ZnS	35 nm	67–73 nm	[26,27]
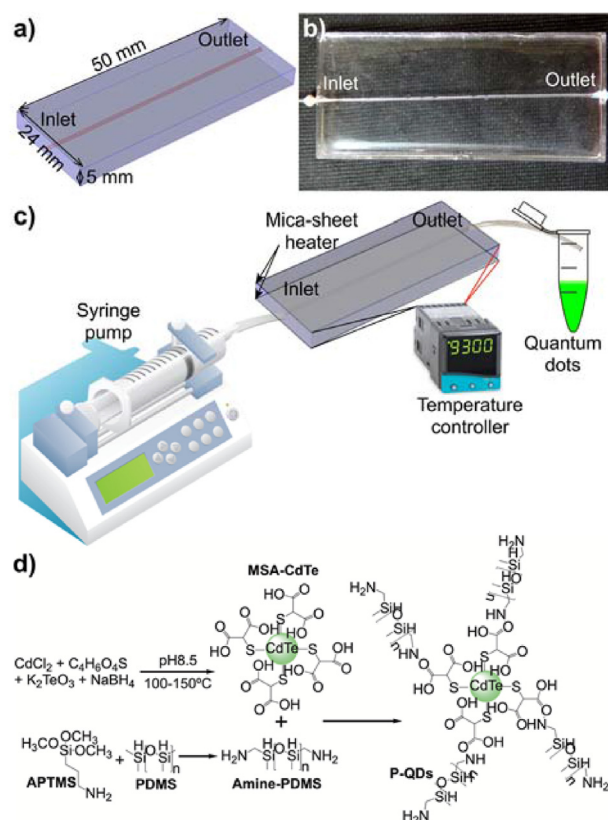
Fig. 1. PDMS microreactor used to synthesize QDs: a) Schematic along with dimensions b) Optical image. c) Schematic of the setup. d) Chemical reactions involved in the synthesis of PDMS coated CdTe quantum dots.

(~250 °C), thus suitable for thermally expensive reactions [32].

For synthesizing size-tunable CdTe QDs, the reaction mixture containing Cd (0.26 g/50 mL), Te (0.014 g/50 mL) salts as a precursor, mercaptosuccinic acid [MSA] (30 mg/mL) as a capping agent, and sodium borohydride [NaBH$_4$] (2 mg/mL) as reducing agent were introduced through the inlet. 1 mL of synthesized QDs were collected from the outlet (Fig. 1c).

Further, to render the cadmium telluride quantum dots (CdTe QDs) biocompatible, PDMS was coated as shown in the scheme (see Fig. 1d). PDMS was modified under oxygen plasma (radiofrequency [RF] power of 60 W for 18 min) to activate hydroxyl groups, followed by the addition of 3-Aminopropyltrimethoxysilane (APTMS) to ensure amine functionalization. A quantity of 100 μL of the amine-functionalized solution was diluted with toluene (1 mL) to guarantee unrestricted flow through the microchannel. Further, 100 μL of the diluted solution was added into the reaction containing cadmium (Cd), tellurium (Te), mercaptosuccinic acid (MSA), and sodium borohydride (NaBH$_4$). The microreactor was held in between two mica heaters to maintain a specific temperature, and a syringe pump was used to set a flow rate (Harvard Apparatus Pump 11 Elite). Finally, synthesized P-QDs were collected through an outlet of the microreactor and purified using ethanol by centrifugation at 10000 rpm for 20 min. The obtained pellet was then suspended in Millipore water and was lyophilized. A stock solution of QDs (1 mg/mL) was made for further experiments.

2.2. Optical and structural characterization

1 mg/mL QDs were dissolved in 1 × phosphate buffer saline (PBS) and characterized by photoluminescence (PL) spectroscopy (Hitachi F-2500). Further, the quantum yield of P-QDs (the process details are provided in the supplementary section 2) was determined using

Rhodamine 6G as standard [33].

The coating of PDMS was confirmed by Fourier transform infrared (FT-IR) spectroscopy (IR Affinity-1, SHIMADZU), followed by size assessment using atomic force microscopy (AFM) and transmission electron microscopy (TEM).

2.3. Toxicity assessment

The cell viability of P-QDs was evaluated by measuring cell growth inhibition using 3-(4,5-dimethylthiazol-2-yl)-2,5-diphenyl tetrazolium bromide (MTT) reagent (Sigma Aldrich). The details of the standard protocol are provided in the Supplementary section 4.

2.4. Ion leaching estimation

Cd^{2+} ion leaching study was carried out using atomic absorption spectroscopy [AAS] (Perkin Elmer-A Analyst 800). Cadmium standards of 1 ppm, 2 ppm, and 3 ppm were prepared to calibrate the instrument. A working concentration of 0.5 mg/mL (P-QDs and bare QDs) was prepared and kept at 37 °C. Further, Cd^{2+} ion leaching was recorded at different time intervals (0–12 h).

2.5. Bio-imaging - in-vitro

For cellular internalization assay, green CdTe QDs were synthesized using conventional (CQDs) and microreactor (MQDs) method. 100 μL of both the QDs was used for internalization experiment from 1 mg/mL stock. HepG2 cells (10^4 cells/well) were seeded into a 6 well plate for the internalization experiment. After reaching 70% confluency, the cells were washed with a serum-free medium. Further, QDs were added in a serum-free medium and incubated for 1 h. Furthermore, the cells were washed (1 × PBS) and fixed using 4% paraformaldehyde, followed by permeabilization using 0.1% TritonX and staining with 4′,6-diamidino-2-phenylindole (DAPI). Finally, the cells were mounted on a thin cover glass and used for imaging.

NIH 3T3 cells were maintained in Dulbecco's Modified Eagle Medium (DMEM) medium with 10% fetal bovine serum (FBS) and appropriate antibiotic condition. NIH 3T3 cells (10^4 cells/well) were seeded and grown on coverslips in 6-well culture plates till they are 70–80% confluent. Further, the cells were washed, followed by fixation using 4% paraformaldehyde. After fixation, cells were washed and permeabilized by 0.1% TritonX-100. Finally, the cells were washed with 1 × PBS and treated with P-QDs conjugates (protocol for conjugation of antibodies is given in supplementary section 5) at a concentration of 6.25 μg/mL for 1 h at 37°C under dark conditions. For control, the cells were treated with Hoechst33342 and Actin green 488 for staining the nucleus and cytoskeleton, respectively. After incubation, the cells were washed thrice with 1× PBS and imaged using a confocal microscope (Leica-SP8).

2.6. Bio-imaging - zebrafish

For zebrafish maintenance and experimentation, the guidelines recommended by the Committee for Control and Supervision of Experiments on Animals (CPCSEA), Govt. of India, were followed. Institute Animal Ethics Committee (IAEC) approved the animal care procedures, and protocols were used in this study.

Animals were anesthetized by immersion into 0.02% tricaine and immobilized by squeezing them ventral upwards into a foam holder mounted on a Petri dish. A small incision was made through the body wall and the pericardium using fine forceps. Once the pericardial sac was opened, the heart ventricle was exposed by gently squeezing the abdomen. A 0.4 mm diameter copper filament linked to a polypropylene insulation tube was cooled in liquid nitrogen and placed on the ventricular surface until thawing could be observed (a few seconds). After the operation, fish were placed in a freshwater tank, and pipe ting system water onto the gills was done for a couple of minutes. Fish were

swimming normally after 30 min. For analysis of proliferation during regeneration, animals were sacrificed at 7 days after injury by immersion in 0.04% tricaine, and hearts were dissected in PBS. Zebrafish were dissected, hearts were isolated and fixed in 4% (vol/vol) paraformaldehyde at room temperature for 1 h. Further, the tissue samples were cryopreserved with 30% (wt/vol) sucrose overnight at 4 °C before immersion in tissue freezing medium (Leica) and were immediately stored at −80°C. For immunofluorescence, cryosections were thawed, air dried, refixed in 4% (vol/vol) paraformaldehyde washed twice using PBS before permeabilization with PBST (1X PBS, 0.5% TritonX-100) at room temperature for 15 min. Samples were then washed twice with PBST and incubated in blocking solution [1 × PBS, 3% (vol/vol) Bovine Serum Albumin, 0.1% TritonX-100]. Primary antibodies conjugated with red and green P-QDs were incubated overnight at 4°C, followed by two PBS washes containing 0.1% NP40 (vol/vol). Slides were rewashed with PBS before mounting with Mowiol mounting medium. Primary antibodies used in this study include anti-myosin heavy chain (MF20; DSHB) conjugated with green QDs at 1:50 and PCNA (Santa Cruz Biotech) conjugated with red QDs at 1:100.

For the dye control experiment, injured hearts were isolated from zebrafish subsequently 4 days after cryo-injury, and cardiac tissue was embedded in a tissue-freezing medium following standard protocols. The heart was sagittally sectioned (10 μm, cryotome, Leica). Immunohistochemical analyses were performed on these tissue sections as described previously [34]. Briefly, PBS-washed tissue sections were re-fixed, permeabilized, blocked, and incubated with primary antibodies (mouse MF20, 1:40 (DSHB, USA); PCNA, 1:100 (Santa Cruz Biotechnology, USA)) overnight at 4 °C after incubating for 1 h in a blocking solution [5% goat serum (MP Biomedicals)/0.2% Tween 20/PBS]. Primary immune complexes were detected by Alexa Fluor™ 488- or Alexa Fluor™ 555- or Alexa Fluor™ 647 phalloidin antibodies (1:400; Molecular Probes). Heart sections were imaged using a Leica-SP8 confocal microscope, and the images were analyzed using LasX software.

3. Results

3.1. Derivation of the mathematical equation using dimensional analysis

To achieve desired properties during nanoparticle synthesis, dependence on individual or several process parameters must be precisely controlled. Such control of individual parameters could be obtained using microreactors. However, to achieve monodispersity in size, precision control of multiple parameters is essential. Thus, we have selected the dimensional analysis approach as a powerful tool applied to multivariate problems to understand their behavior and interpret complex interactions of variables [35]. It generalizes the parameters and results in a dimensionless mathematical form with the minimum number of experiments [36]. Thus, an equation can be derived that can accurately predict process parameters required to synthesize monodispersed quantum dots.

To derive an equation, parameters such as flow rate (f), Temperature (T), and Cd/Te ratio (R) were considered as significant variables affecting the size of QDs (detail of dimensional analysis method is provided in section 1 of the supplementary information). Based on these significant variables, experiments were performed by varying individual parameters to obtain boundary conditions for the synthesis. Table S1 of the supplementary information summarizes the parameters used along with boundary conditions.

Based on the process parameters generated by the design of experiments (refer to Table S2 of supplementary information), CdTe QDs were synthesized in a continuous flow active microreactor, and their PL values were recorded. The emission maxima of QDs can be correlated to the size by inserting the peak value (λ) obtained from the PL data in the equation reported by Yu et al. [37].

$$Size(nm) = 9.8127 \times 10^{-7}\lambda^3 - 1.7147 \times 10^{-3}\lambda^2 + 1.0164\lambda - 194.84 \qquad (1)$$

The polynomial equation given by Yu et al. is limited to emission maxima of 450 nm. Therefore, we have modified the equation based on the data obtained in our study to fit the values of emission maxima below 450 nm. The obtained results (refer to Table S2 of supplementary information) suggest that the size of QDs is relational to the chosen parameters (*f*, *T*, and *R*) and, therefore, can be expressed as eq. (2).

$$S_{QD} = Kf^a T^b R^c \qquad (2)$$

where S_{QD} is the size of QDs, *f* is the flow rate, *T* is the temperature, *R* is the Cd/Te ratio, *a*, *b* and *c* are respective exponents, and *K* is the proportionality constant.

Total of 15 experiments were performed (see Table S2 for details of the parameters used), and QDs thus synthesized were characterized by PL. The results were analyzed by fitting the power line equation, and the values of exponents and proportionality constant were determined: $a = -0.038$, $b = -0.019$, $c = -0.082$, and $K = 669.61$. Substituting these values, eq. (2) can be rewritten as:

$$S_{QD} = 669.61 f^{-0.038} T^{-0.019} R^{-0.082} \qquad (3)$$

The above equation suggests that higher the exponent value, the greater is the influence of that parameter on the synthesis process. Therefore, the order of significance for the synthesis of QDs can be written as: temperature > flow rate > Cd/Te ratio. The value of 669.61 obtained for *K* nullifies any errors introduced during the synthesis.

Further, the equation was validated using the parameters predicted for a given size value (refer to Table S3 of supplementary information). Accuracy in the prediction of size was >95% for a predetermined value. The details which are given in Table S3 of the supplementary information.

The validated dimensionless mathematical equation was utilized to synthesize QDs of four different sizes viz. 0.23 nm, 3.24 nm, 3.42 nm, and 4.34 nm emitting blue, green, yellow, and orange, respectively. Table 2 provides experimental conditions obtained from the eq.(3) to synthesize QDs of four target sizes as well as corresponding results from PL (size calculated from eq. (1)) and AFM along with the coefficient of variance (CV). CV was calculated by the nanocluster method ($CV = \sigma/d$ where σ and *d* are the standard deviation and mean size respectively) reported by Sun et al. According to Sun et al. [38], CV provides a stringent measure of monodispersity and should be preferred over standard deviation (SD).

The variance of <5% was calculated for the results obtained from PL (except for the target size of 0.23 nm). Whereas variance of <8% is determined for the results obtained from AFM. Further, the accuracy of prediction of size was obtained to be >95% using a formula given in supplementary information. The AFM (Fig. 2a–d) shows the 3D topography of QDs synthesized using the derived parameters and its size distribution chart (2D image and line profile is given in Fig. S1 of supplementary information). The particle sizes (0.5–3.92 nm) derived from the AFM indicate monodispersed preparation, as the calculated CV was <8%.

Fig. 2e shows PL spectra displaying size-tunable emission when excited at 350 nm. TEM for green (550 nm) colored QDs (Fig. 2f) shows nanoparticles of the size range 3–5 nm, which agrees reported literature [39,40].

Thus, it could be deduced that the dimensional analysis, in conjunction with the microreactor, yields monodispersed QDs. Further, for bio-
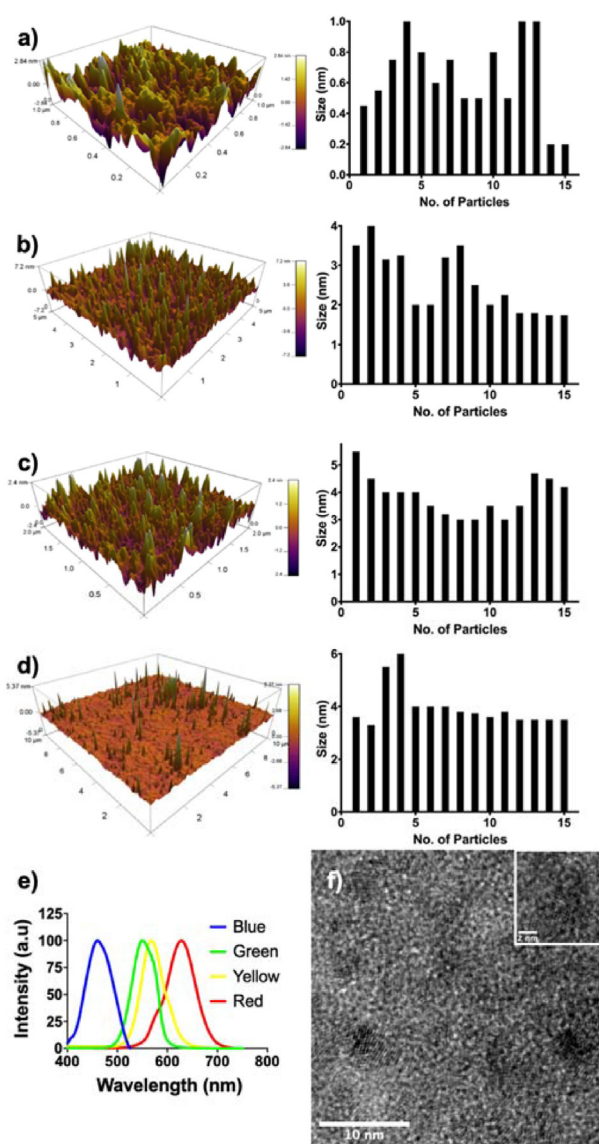

Fig. 2. AFM 3D topographic images and size distribution graph different sized QDs of a) 0.5 nm; b) 3.32 nm; c) 3.34 nm; and d) 3.92 nm; e) Photoluminescence spectra of all the QDs; f) TEM of green-colored CdTe nanoparticles are seen in a size range of 3–5 nm (atomic planes are visible in the inset image).

imaging application, CdTe QDs need to be rendered biocompatible. Thus, polydimethylsiloxane (PDMS) elastomer was coated on CdTe QDs (P-QDs) synthesized using mathematically derived process parameters in a continuous flow active microreactor.

3.2. Synthesis and characterization of PDMS coated QDs

CdTe QDs of five different colors (blue, green, yellow, orange, and red) were synthesized in a continuous flow active microreactor using the

Table 2
Predicted process parameters for synthesizing QDs of four target sizes. The resultant size by PL and AFM is given along with the calculated CV.

Target Size (nm)	Predicted Process Parameters			Obtained size (nm) and coefficient of variation (%)			
	Ratio (Cd:Te)	Temperature (°C)	Flow rate (μL/min)	Calculated by eq. 3	CV	AFM	CV
0.23	8	200	500	1.31	23.4	0.5	7.1
3.24	4	90	85	3.13	2.4	3.32	5.1
3.42	4	90	26	3.37	1.8	3.34	6.9
4.34	1	100	21	3.96	4.1	3.92	2.8

optimized parameters obtained from eq. (3) and were coated with PDMS. As PDMS is thermally stable with a flashpoint of ~321°C [41], the synthesis temperature of 200 °C doesn't affect the coating quality.

The FTIR spectrum of CdTe (given in Fig. 3a) display peaks at 925 cm^{-1}, 1061 cm^{-1}, 1410 cm^{-1}, 2293 cm^{-1}, 2541 cm^{-1}, and 3544 cm^{-1} corresponding to C–O vibration, C–O stretching, C–H, C=C, O–CH$_3$ stretching vibration, and free OH respectively. FT-IR spectrum of P-QDs show all the characteristic peaks of CdTe in addition to peaks at 950 cm^{-1}, 1000 cm^{-1}, and a broad peak from 1352 to 1455 cm^{-1} corresponding to Si–O–Si, Si–O–CH$_3$, and Si–O–CH$_2$CH$_3$, respectively indicating the presence of PDMS. Moreover, a peak at 1598 cm^{-1},
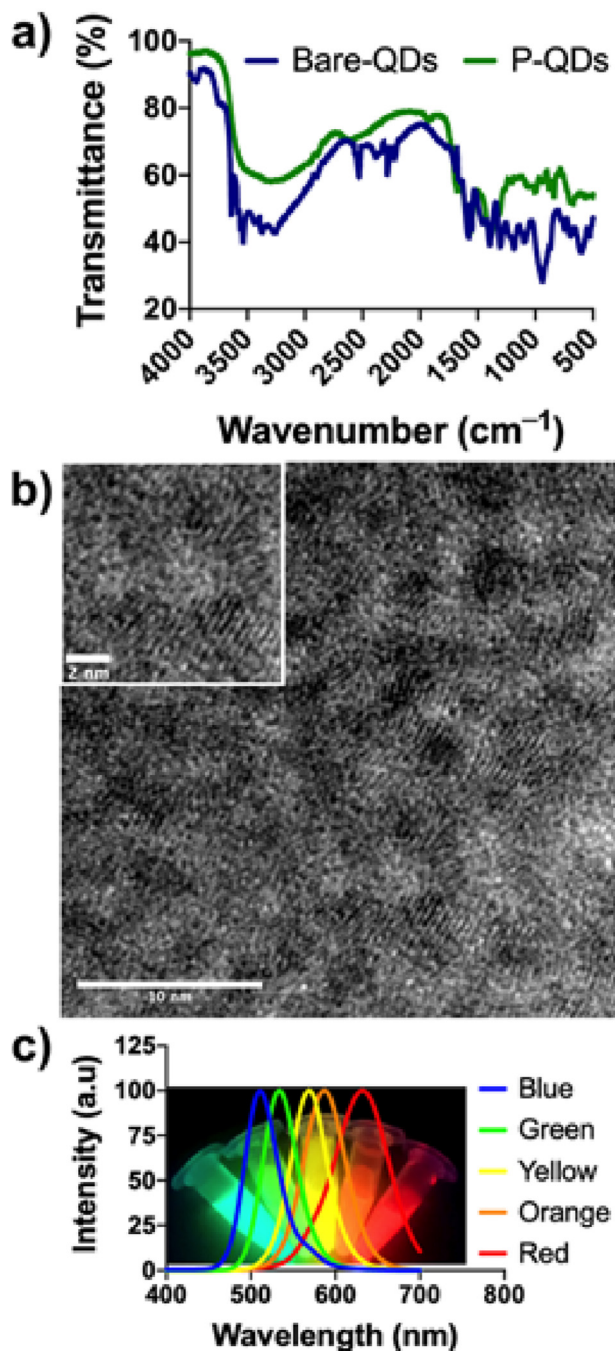
corresponding to NH stretch of primary amine, indicate amine modification of PDMS. The broad peak at 3500 cm^{-1} corresponds to NH from amine modification and free OH.

TEM micrograph provided in Fig. 3b reveals the size of P-QDs to be ~5 nm. The inset shows an expanded region of the micrograph with atomic planes. The diffused area of the image compared to bare CdTe (see Fig. 2f) is due to PDMS coating.

PL spectra (Fig. 3c) show emission peaks at 500 nm, 534 nm, 570 nm, 588 nm, and 630 nm (blue, green, yellow, orange, and red). Quantum yield (QY) of P-QDs and bare QDs was calculated from PL to be 61.5% and 24.2%, respectively (for details, please refer to Fig. S2, S3 and Table S5 of the supplementary section 2). Higher QY compared to bare CdTe QDs can be attributed to the siloxane polymer matrix [42]. Moreover, polymer coating imparts enhanced photostability (~44%) as compared to the bare QDs (23%), which was assessed by continuous exposure to UV (4W) for 96 min (refer to Fig. S4 of the supplementary section). Hoechst33342 (used as a fluorescent dye control) degraded significantly under similar exposure, yielding photostability of 14%. These results suggest that the Si–O layer of PDMS may prevent the loss of excitons, leading to superior photostability [43].

3.3. Cytotoxicity assessment

The cytotoxicity of QDs was evaluated by the effect on the cell viability by MTT assay. The reduction in viability of NIH 3T3 cells treated with different concentrations of P-QDs and bare QDs is presented in Fig. 4a. P-QDs were less toxic at a concentration of 6.25 μg/mL (cell viability >80%) [44]. Whereas bare QDs were toxic at all the concentrations due to leaching of Cd^{2+} ions. Ion leaching profile (Fig. 4b) up to 12 h by AAS indicated a significantly low release of Cd^{2+} ions from P-QDs (1.54 ppm) compared to the bare ones (3.67 ppm).

3.4. Bio-imaging – in-vitro

Confocal microscopy data (see Fig. 5) reveals internalization (near the nucleus) of both the QDs in HepG2 cells. However, observation of the green intensity shows a greater number of internalized MQDs as compared to CQDs. Further, images were analyzed using the "Intracellular nanoparticle uptake (IntraCell V2)" tool available in ImageJ software. Images of green-colored QDs and a blue-stained nucleus were used for the analysis. The number of QDs internalized per cell was calculated to be 136 and 47 for MQDs and CQDs, respectively (see supplementary section 5 for details of the analysis). This suggests that the monodispersed QDs synthesized using microreactor were internalized significantly more than conventionally synthesized QDs. Moreover, the number of QDs visible outside the cells are less in the case of MQDs. A 3D image (see Fig. S6 of supplementary information) reveals an accumulation of small-sized monodispersed MQDs (~5 nm) within the nucleus. The probable mechanism of the nuclear uptake of MQDs is passive diffusion via water channels (~9 nm) of the nuclear pore complex [45,46].
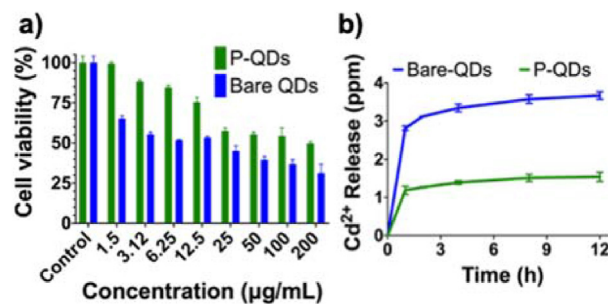

Fig. 3. a) FT-IR spectra of bare CdTe and PDMS coated CdTe QDs. b) TEM showing uniformly dispersed P-QDs with the size of ~3–5 nm. The inset of the image shows an enlarged image revealing atomic planes. c) Photoluminescence spectra recorded at an excitation wavelength of 320 nm. The background picture shows different colored P-QDs.

Fig. 4. a) Cytotoxicity studies with NIH 3T3 cells indicate biocompatibility of P-QDs at a dose of 6.25 μg/mL b) Time-dependent ion leaching studies show low Cd^{2+} release from P-QDs as compared to bare counterparts.
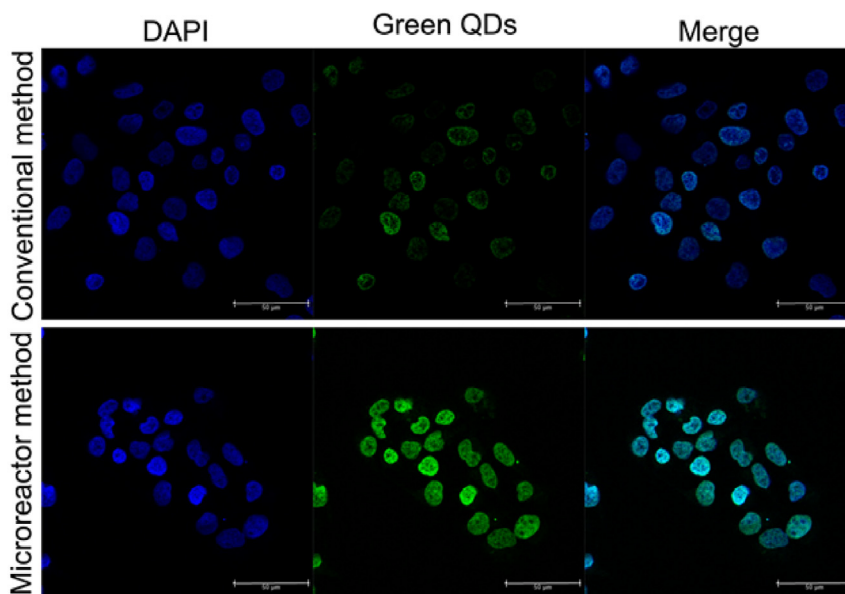
Fig. 5. Confocal microscopic images of conventional and microreactor synthesized QDs internalized in HepG2 cells. DAPI is used for staining the nucleus. The excitation wavelength used for visualizing DAPI and QDs was 405 nm. Scale bar: 50 μm; Magnification: 63×.

P-QDs of two different sizes corresponding to blue and green emission wavelengths were used to demonstrate multiplexed bio-imaging. Blue and green QDs were conjugated to SMAR-1 protein and smooth muscle actin antibody, respectively, with the efficiency >74% (refer to Fig. S7 and Table S6 of supplementary section 6). NIH 3T3 cells were treated with QD-conjugates and imaged using a confocal microscope. Both the conjugates can be seen bound to their target sites under the confocal microscope using a single excitation wavelength of 405 nm (Fig. 6).

3.5. Bio-imaging - zebrafish

For immunohistostaining, AlexaFluor 488 and AlexaFluor 647 phalloidin conjugated antibodies were used to stain MF-20 and PCNA, respectively. The primary antibodies should be derived from different hosts to achieve specific labelling by fluorophore-conjugated

Fig. 6. Confocal microscopic images of NIH 3T3 cells. Hoechst 33342 (360/460) and Actin Green (495/518) were used as a control to stain the nucleus and cytoskeleton, respectively, and captured sequentially. Blue and green QDs were conjugated with SMAR-1 nucleus-specific protein and smooth muscle actin antibodies to target and cytoskeleton, respectively. The bottom panel was captured simultaneously at an excitation wavelength of 405 nm. Scale bar: 10 μm; Magnification: 63×.

secondary antibodies [34]. However, in the dye control image panel of Fig. 7, the primary antibodies for MF20 and PCNA are derived from the same host (mouse). Thus, the imaging of both antibodies was done separately to avoid undifferentiated labelling. To visualize the proliferation of the cells after the injury, AlexaFluor 555 phalloidin stain was used along with AlexaFluor 647 phalloidin antibody specific to PCNA. AlexaFluor 555 phalloidin stains the cytoskeleton of the cells non-specifically.
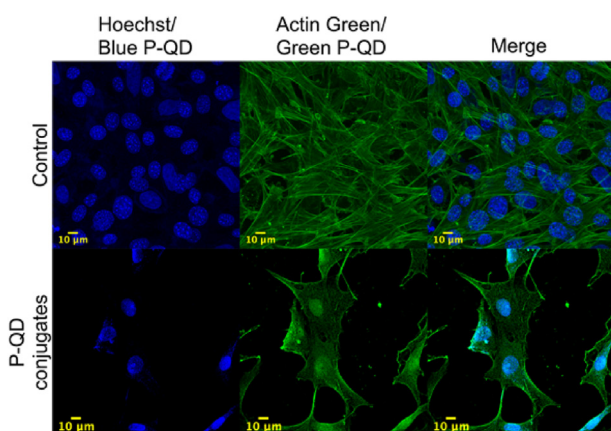
On the other hand, QDs can be conjugated to the primary antibody without secondary antibodies. Thus, in our study, QDs were conjugated to both the antibodies (MF20 and PCNA) and multiplexed imaging was carried out at a single excitation wavelength of 405 nm.

To carry out the multiplexed bio-imaging of P-QDs in zebrafish, green and red P-QDs were conjugated to MF20 and PCNA antibodies, respectively, with a conjugation efficiency of >65% (refer to Fig. S7 and Table S6 of supplementary section 6). The conjugates were introduced to the cardiac tissue sections of zebrafish and were imaged using confocal microscopy. Green and red P-QD conjugates (on simultaneous observation) were found to target specifically their respective regions in the tissue, which was confirmed by confocal microscopy (Fig. 7). In Fig. 7, red fluorescence in the region of regenerating cells can be seen specifying the localization of red P-QDs tagged antibodies. Similarly, green fluorescence in the region of cardiac tissue indicates the localization of green P-QDs. Additionally, there was no fluorescence reduction observed under prolonged UV exposure during confocal microscopy owing to photostability. Thus, the candidature of P-QDs for multiplexed bio-imaging applications can be justified.

To demonstrate the superiority of P-QDs over the fluorescent dyes, intensities of red-colored P-QDs and AlexaFluor 647 phalloidin were analyzed using ImageJ software (see Fig. S8 of supplementary section 7 for the details of image analysis). The analysis reveals significantly higher intensities of P-QDs (see bar graph in the dye control panel of Fig. 7), with a marginal increase in area.

4. Discussion

QDs are extensively used in various applications due to the display of exceptional properties, specifically, photostability and narrow size-tunable emission. To date, these properties, along with
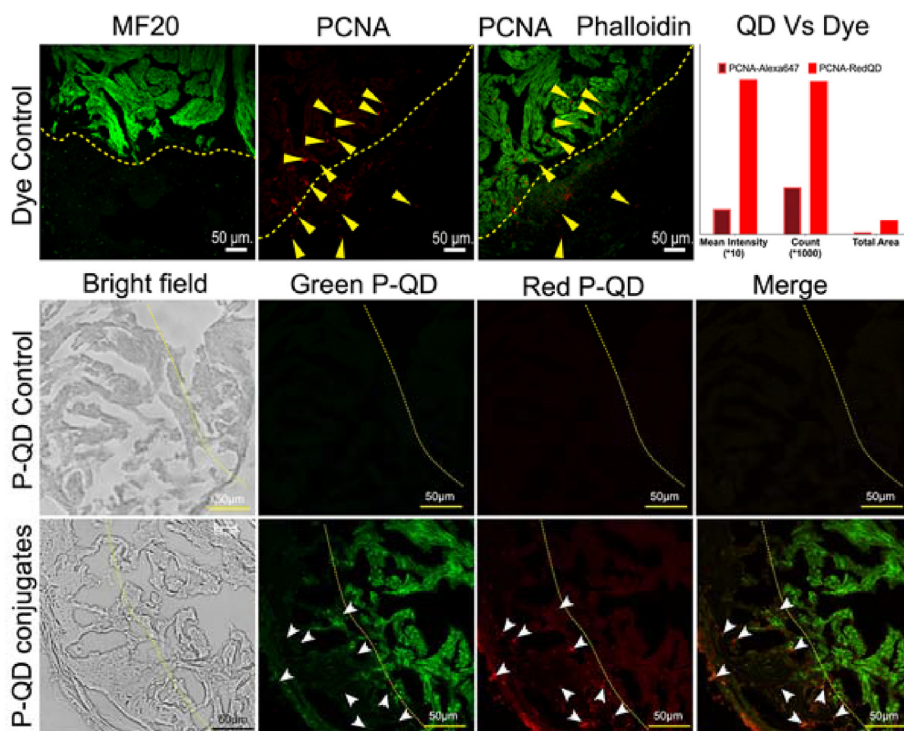
Fig. 7. Confocal images of sagittal cardiac sections showing cardiomyocytes and proliferating cells in wild-type zebrafish cardiac tissue. The dye control panel shows Alexa Fluor 488-phalloidin and Alexa Fluor 647-phalloidin conjugated with primary antibodies of MF20 and PCNA, respectively. The overlay image shows Alexa Fluor 555 Phalloidin (Green) and Alexa Fluor 647-phalloidin conjugated with PCNA primary antibody. A comparison of fluorescence intensities of QDs and dyes analyzed using ImageJ software is shown as a bar chart. PQDs control panel represents confocal images stained with unconjugated green and red P-QDs as a negative control. Green P-QDs conjugated MF20, and red P-QDs conjugated PCNA recognize cardiomyocytes and nuclei undergoing DNA synthesis. Arrowheads point to the proliferating cells in the injury region (for dye control and QDs). The yellow dotted line (for dye control and QDs) demarcates the healthy cardiac tissue from the cryo-injured region. The images with the dye were captured after 4 dpci, whereas those with QDs were imaged after 7 dpci. Scale bar: 50 μm; Magnification: 63×.

biocompatibility [3,47] have been achieved by employing conventional synthesis methods.

In the present work, the synthesis parameters were predicted by deriving a dimensionless mathematical equation to obtain high-quality CdTe QDs. Dimensional analysis works on the assumption that process parameters affect discretely and/or collectively the output of the reaction and thus solve complex inter-parametric interactions by applying a multivariate approach [28,35]. The analysis not only provides the order of significance of variables affecting synthesis but also enables precision in the prediction of parameters to achieve reproducibility. Micro reaction technology, known to produce high-quality output owing to its numerous advantages, was utilized in conjunction with a dimensional analysis approach to yield monodispersed QDs.

Thus, synthesis parameters were predicted using a dimensionless mathematical equation (eq. (3)), and CdTe quantum dots were synthesized in a continuous flow active microreactor. AFM data showed a CV of <8% to synthesize four target sizes with a parameter prediction accuracy of >95% (see Table S3 of supplementary information). FWHM of ~40 nm was calculated from PL data for the microreactor synthesized CdTe QDs at an emission maximum of 540 nm (refer to Fig. S2 of supplementary information). Whereas FWHM of ~50 nm was recorded for the conventionally synthesized QDs, proving the superiority of the microreactor-based synthesis process in terms of monodispersity.

Further, the conventionally synthesized QDs (CQDs) and microreactor synthesized QDs (MQDs) were assessed for bio-imaging application. Both the QDs were subjected to HepG2 cells (Fig. 5) and allowed to internalize. More MQDs (136/cell) were internalized and seen closer to the nucleus. Few MQDs were even spotted within the nucleus. The probable mechanism of the uptake of these QDs might be via the water channels of the nuclear pore complex owing to their small size and monodispersed nature [45,46].

Moreover, reproducibility in the synthesis of QDs was recorded from 2015 to 2021 (see Table S4 of the supplementary information for details). On average, a newly fabricated microreactor was used after every fourth experiment. Size and FWHM were estimated from the PL spectrum for all the samples. Emission maximum of ~550 nm was kept constant for the calculation. CV of ~2.4% and ~9% were recorded for the size and FWHM, respectively. The value of CV <5% in size shows a high degree of

reproducibility. Moreover, the variance of size distribution data (FWHM) for multiple experiments was ~9%, indicating monodispersed synthesis.

To render the QDs biocompatible, PDMS was covalently bonded on the surface of the nanocrystals (Fig. 1d), which is confirmed by the presence of 1000 cm^{-1} (Si–O bond) and 1598 cm^{-1} (NH stretch of amine) recorded from FT-IR (Fig. 3a). As seen from the TEM (Fig. 3b), P-QDs are uniformly dispersed in the PDMS matrix, evident from the diffused micrograph. The coated QDs are quantum efficient (PLQY: 61.5%) and stable (~44%) as compared to the bare ones (PLQY: 24.2%; stability: 23%). The increment in quantum efficiency and photostability can be attributed to covalent bonding of the core (CdTe) and the shell (PDMS) [42,48] as well as uniform dispersion of QDs in the matrix.

Due to the covalent bonding between CdTe and the PDMS, the energy levels overlap, giving rise to core/shell electronic energy levels with a lower bandgap than the bare CdTe. Further, the bonding causes delocalization of core/shell lowest unoccupied molecular orbital (LUMO) throughout the structure and the highest occupied molecular orbital (HOMO) to the core. This phenomenon will decrease the electronic transfer's overall energy and confine the holes to the core [48]. This confinement will ensure less energy required for the radiative electron transfer from HOMO to LUMO, contributing to higher QY. Furthermore, the confinement of holes to the core reduces the possibility of interaction at the surface, thus, increasing the stability of P-QDs [49]. Less leaching of Cd^{2+} ions from P-QDs (Fig. 4b) can thus be attributed to this confinement, rendering them biocompatible [44].

P-QDs were further used for multiplexed imaging *in-vitro* and cardiac tissue of zebrafish. The polymer coating readily allows the conjugation of biomarkers for targeting specific organelle. P-QDs of different sizes were employed as an imaging agent to target cellular organelles such as the nucleus and cytoskeleton of NIH 3T3 cells. An advantage to utilize QDs for multiplexed imaging is their capability to emit several colors (size tunability) at a particular excitation wavelength. P-QDs were localized to their targeted organelles; however, owing to the conjugation efficiency (~75%), non-specific distribution was observed (Fig. 6). The presence of few P-QDs outside the organelle can be attributed to the size of the polymer matrix [50].

Likewise, fluorescent dyes and P-QDs were conjugated with PCNA and MF20 biomarkers for understanding the regeneration of cells after

the injury to the cardiac tissue of zebrafish (Fig. 7). Dyes could not be used for simultaneous imaging as they need to be conjugated with secondary antibodies possessing serious constraints of specificity. Further, due to the use of antibodies, the overall process is costly. However, as P-QDs exhibit multiple emission spectra at a single excitation wavelength, they could be imaged simultaneously. Specific primary antibodies can be conjugated to QDs owing to the surface modification, thus obviating the use of a secondary antibody. Moreover, QDs exhibit intense fluorescence and photostability for a longer period, compared to the dyes, thus suitable for multiplexed bio-imaging.

5. Conclusion

The continuous flow active microreactor-based synthesis, in conjunction with mathematically predicted process parameters, was employed to obtain narrow size-tunable monodispersed QDs with a high degree of reproducibility. Further, the synthesized QDs were rendered biocompatible by coating with PDMS. The coating not only provided biocompatibility but also enhanced quantum efficiency and photostability. Lowering the Cd^{2+} leaching proved the effect of the coating. These P-QDs were then successfully demonstrated for their application in multiplexed bio-imaging for *in-vitro* and zebrafish tissue. The developed synthesis strategy is effective in obtaining high-quality quantum dots reliably. Thus, the methodology (microreactor in conjunction with dimensionless mathematical equation) can be made industry viable by process automation, solving the perennial problem in synthesizing monodispersed, quantum efficient, and photostable polymer-coated quantum dots.

Credit author statement

Sulaxna Pandey conducted experiments on synthesis of quantum dots, their characterization and in vitro studies. Dhananjay Bodas conducted the experiments on zebrafish. Pranav Kshirsagar was instrumental in employing dimensional analysis method. Chinmoy Patra conceptualized the work on zebrafish and analyzed the same. Dhananjay Bodas conceptualized the complete study from synthesis of monodispersed, reproducible, high quality quantum dots to multiplexed imaging studies and analysis.

Declaration of competing interest

The authors declare that they have no known competing financial interests or personal relationships that could have appeared to influence the work reported in this paper.

Acknowledgment

Appendix A. Supplementary data

Supplementary data to this article can be found online at https:// doi.org/10.1016/j.mtbio.2021.100123.

References

[1] R. Koole, E. Groeneveld, D. Vanmaekelbergh, A. Meijerink, C. de Mello Donegá, Size effects on semiconductor nanoparticles, in: Nanoparticles, Springer Berlin Heidelberg, Berlin, Heidelberg, 2014, pp. 13–51, https://doi.org/10.1007/978-3-662-44823-6_2.

[2] A.M. Iga, J.H.P. Robertson, M.C. Winslet, A.M. Seifalian, Clinical potential of quantum dots, J. Biomed. Biotechnol. 2007 (2007) 1–10, https://doi.org/10.1155/2007/76087.

[3] S. Pandey, D. Bodas, High-quality quantum dots for multiplexed bioimaging: a critical review, Adv. Colloid Interface Sci. 278 (2020) 102137, https://doi.org/10.1016/j.cis.2020.102137.

[4] R. Girija Aswathy, B. Sivakumar, D. Brahatheeshwaran, T. Ukai, Y. Yoshida, T. Maekawa, S.D. Kumar, Biocompatible fluorescent jelly quantum dots for bioimaging, Mater. Express. 1 (2011) 291–298, https://doi.org/10.1166/mex.2011.1045.

[5] H. Cui, R. Wang, Y. Zhou, C. Shu, F. Song, W. Zhong, Dual-function fluorescent probe for cancer imaging and therapy, Luminescence 31 (2016) 813–820, https://doi.org/10.1002/bio.3028.

[6] I.V. Martynenko, A.P. Litvin, F. Purcell-Milton, A.V. Baranov, A.V. Fedorov, Y.K. Gun'ko, Application of semiconductor quantum dots in bioimaging and biosensing, J. Mater. Chem. B. 5 (2017) 6701–6727, https://doi.org/10.1039/C7TB01425B.

[7] Q. Zhang, J. Xie, Y. Yu, J.Y. Lee, Monodispersity control in the synthesis of monometallic and bimetallic quasi-spherical gold and silver nanoparticles, Nanoscale 2 (2010) 1962, https://doi.org/10.1039/c0nr00155d.

[8] M. Muzzio, J. Li, Z. Yin, I.M. Delahunty, J. Xie, S. Sun, Monodisperse nanoparticles for catalysis and nanomedicine, Nanoscale 11 (2019) 18946–18967, https://doi.org/10.1039/C9NR06080D.

[9] A.M. Nightingale, J.C. de Mello, Microscale synthesis of quantum dots, J. Mater. Chem. 20 (2010) 8454, https://doi.org/10.1039/c0jm01221a.

[10] S.-Y. Jung, Y. Liu, C.P. Collier, Fast mixing and reaction initiation control of single-enzyme kinetics in confined volumes, Langmuir 24 (2008) 4439–4442, https://doi.org/10.1021/la800053e.

[11] Y. Cheng, S. Da Ling, Y. Geng, Y. Wang, J. Xu, Microfluidic synthesis of quantum dots and their applications in bio-sensing and bio-imaging, Nanoscale Adv. (2021) 2180–2195, https://doi.org/10.1039/d0na00933d.

[12] R. Kikkeri, P. Laurino, A. Odedra, P.H. Seeberger, Synthesis of carbohydrate-functionalized quantum dots in microreactors, Angew. Chem. Int. Ed. 49 (2010) 2054–2057, https://doi.org/10.1002/anie.200905053.

[13] J. Wang, H. Zhao, Y. Zhu, Y. Song, Shape-controlled synthesis of CdSe nanocrystals via a programmed microfluidic process, J. Phys. Chem. C 121 (2017) 3567–3572, https://doi.org/10.1021/acs.jpcc.6b10901.

[14] H.E. Grecco, K.A. Lidke, R. Heintzmann, D.S. Lidke, C. Spagnuolo, O.E. Martinez, E.A. Jares-Erijman, T.M. Jovin, Ensemble and single particle photophysical properties (two-photon excitation, anisotropy, FRET, lifetime, spectral conversion) of commercial quantum dots in solution and in live cells, Microsc. Res. Tech. 65 (2004) 169–179, https://doi.org/10.1002/jemt.20129.

[15] S. Marre, J. Baek, J. Park, M.G. Bawendi, K.F. Jensen, High-pressure/high-temperature microreactors for nanostructure synthesis, J. Assoc. Lab. Autom. 14 (2009) 367–373, https://doi.org/10.1016/j.jala.2009.06.005.

[16] S. Kubendhiran, Z. Bao, K. Dave, R.-S. Liu, Microfluidic synthesis of semiconducting colloidal quantum dots and their applications, ACS Appl. Nano Mater. 2 (2019) 1773–1790, https://doi.org/10.1021/acsanm.9b00456.

[17] C. Richard, R. McGee, A. Goenka, P. Mukherjee, R. Bhargava, On-demand milifluidic synthesis of quantum dots in digital droplet reactors, Ind. Eng. Chem. Res. 59 (2020) 3730–3735, https://doi.org/10.1021/acs.iecr.9b04230.

[18] J. Wang, H. Zhao, Y. Zhu, Y. Song, Shape-controlled synthesis of CdSe nanocrystals via a programmed microfluidic process, J. Phys. Chem. C 121 (2017) 3567–3572, https://doi.org/10.1021/acs.jpcc.6b10901.

[19] L. Hong, T.L. Cheung, N. Rao, Q. Ouyang, Y. Wang, S. Zeng, C. Yang, D. Cuong, P.H.J. Chong, L. Liu, W.C. Law, K.T. Yong, Millifluidic synthesis of cadmium sulfide nanoparticles and their application in bioimaging, RSC Adv. 7 (2017) 36819–36832, https://doi.org/10.1039/c7ra05401g.

[20] H. Yang, W. Luan, R. Cheng, H. Chu, S.T. Tu, Synthesis of quantum dots via microreaction: structure optimization for microreactor system, J. Nanoparticle Res. 13 (2011) 3335–3344, https://doi.org/10.1007/s11051-011-0247-9.

[21] Peter Robert Gonsalves, The Design and Fabrication of a Microfluidic Reactor for Synthesis of Cadmium Selenide Quantum Dots Using Silicon and Glass Substrates, 2012.

[22] I.M.A. Viegas, B.S. Santos, A. Fontes, G.A. De Lima Pereira, C.F. Pereira, Multivariate optimization of optical properties of CdSe quantum dots obtained by a facile one-pot aqueous synthesis, Inorg. Chem. Front. 6 (2019) 1350–1360, https://doi.org/10.1039/c9qi00105k.

[23] S.G. Pedro, C.S. Martínez-Cisneros, M. Puyol, J. Alonso-Chamarro, Microreactor with integrated temperature control for the synthesis of CdSe nanocrystals, Lab Chip 12 (2012) 1979, https://doi.org/10.1039/c2lc00011c.

[24] J. Cheng, D. Li, T. Cheng, B. Ren, G. Wang, J. Li, Aqueous synthesis of high-fluorescence CdZnTe alloyed quantum dots, J. Alloys Compd. 589 (2014) 539–544, https://doi.org/10.1016/j.jallcom.2013.11.207.

[25] R. Zeng, T. Zhang, J. Liu, S. Hu, Q. Wan, X. Liu, Z. Peng, B. Zou, Aqueous synthesis of type-II CdTe/CdSe core-shell quantum dots for fluorescent probe labeling tumor cells, Nanotechnology 20 (2009), https://doi.org/10.1088/0957-4484/20/9/095102.

[26] B.H. Kwon, K.G. Lee, T.J. Park, H. Kim, T.J. Lee, S.J. Lee, D.Y. Jeon, Continuous in situ synthesis of ZnSe/ZnS core/shell quantum dots in a microfluidic reaction system and its application for light-emitting diodes, Small 8 (2012) 3257–3262, https://doi.org/10.1002/smll.201200773.

[27] C. Wang, S. Xu, Y. Wang, Z. Wang, Y. Cui, Aqueous synthesis of multilayer Mn: ZnSe/Cu:ZnS quantum dots with white light emission, J. Mater. Chem. C 2 (2014) 660–666, https://doi.org/10.1039/c3tc31602e.

[28] P.-H. Yen, J.-C. Wang, Power generation and electric charge density with temperature effect of alumina nanofluids using dimensional analysis, Energy Convers. Manag. 186 (2019) 546–555, https://doi.org/10.1016/j.enconman.2019.03.005.

[29] C. Balocco, A non-dimensional analysis of a ventilated double façade energy performance, Energy Build. 36 (2004) 35–40, https://doi.org/10.1016/S0378-7788(03)00086-0.

[30] S.L. Lee, R.T. Lahey, O.C. Jones, The prediction of two-phase turbulence and phase distribution phenomena using a K-κ model, Japanese J. Multiph. Flow 3 (1989) 335–368, https://doi.org/10.3811/jjmf.3.335.

[31] V. Kamat, I. Marathe, V. Ghormade, D. Bodas, K. Paknikar, Synthesis of monodisperse chitosan nanoparticles and in situ drug loading using active microreactor, ACS Appl. Mater. Interfaces 7 (2015) 22839–22847, https://doi.org/10.1021/acsami.5b05100.

[32] T.S. Radhakrishnan, Thermal degradation of poly(dimethylsilylene) and poly(tetramethyldisilylene-co-styrene), J. Appl. Polym. Sci. 99 (2006) 2679–2686, https://doi.org/10.1002/app.22813.

[33] M.W. Allen, Measurement of Fluorescence Quantum Yields - Technical Note 52019, 2010.

[34] C. Patra, Z. Kontarakis, H. Kaur, A. Rayrik, The zebrafish ventricle : a hub of cardiac endothelial cells for in vitro cell behavior studies, 2017, pp. 1–11, https://doi.org/10.1038/s41598-017-02461-1.

[35] M. Bonert, B.A. Saville, A non-dimensional analysis of hemodialysis, Open Biomed. Eng. J. 4 (2010) 138–155, https://doi.org/10.2174/1874120701004010138.

[36] J.I. Prieto, A.B. Stefanovskiy, Dimensional analysis of leakage and mechanical power losses of kinematic Stirling engines, Proc. Inst. Mech. Eng. Part C J. Mech. Eng. Sci. 217 (2003) 917–934, https://doi.org/10.1243/095440603322310459.

[37] W.W. Yu, L. Qu, W. Guo, X. Peng, Experimental determination of the extinction coefficient of CdTe, CdSe, and CdS nanocrystals, Chem. Mater. 15 (2003) 2854–2860, https://doi.org/10.1021/cm034081k.

[38] S. Sun, Monodisperse FePt nanoparticles and ferromagnetic FePt nanocrystal superlattices, Science (80-.) 287 (2000) 1989–1992, https://doi.org/10.1126/science.287.5460.1989.

[39] V. Poderys, M. Matulionyte, A. Selskis, R. Rotomskis, Interaction of water-soluble CdTe quantum dots with bovine serum Albumin, Nanoscale Res. Lett. 6 (2010) 2–7, https://doi.org/10.1007/s11671-010-9740-9.

[40] S. D' Souza, E. Antunes, T. Nyokong, Synthesis and photophysical studies of CdTe quantum dot-monosubstituted zinc phthalocyanine conjugates, Inorg. Chim. Acta. 367 (2011) 173–181, https://doi.org/10.1016/j.ica.2010.12.027.

[41] S. Aldrich, Material Safety Data Sheet - PDMS 1546300, 2020.

[42] E. Nam, C. Lee, S.J. Kim, H.K. Chung, H. Chae, Stability and dispersion improvement of quantum-dot films by hydrosilylation between quantum-dot ligands and a siloxane matrix, Opt Express 27 (2019) 20037, https://doi.org/10.1364/OE.27.020037.

[43] S.B. Rizvi, S. Ghaderi, M. Keshtgar, A.M. Seifalian, Semiconductor quantum dots as fluorescent probes for in vitro and in vivo bio-molecular and cellular imaging, Nano Rev. 1 (2010) 5161, https://doi.org/10.3402/nano.v1i0.5161.

[44] X. Chen, Z. Guo, P. Miao, One-pot synthesis of GSH-Capped CdTe quantum dots with excellent biocompatibility for direct cell imaging, Heliyon 4 (2018), e00576, https://doi.org/10.1016/j.heliyon.2018.e00576.

[45] M. Havrdová, I. Urbančič, K. Bartoň Tománková, L. Malina, J. Štrancar, A.B. Bourlinos, Self-targeting of carbon dots into the cell nucleus: diverse mechanisms of toxicity in NIH/3T3 and L929 cells, Int. J. Mol. Sci. 22 (2021) 5608, https://doi.org/10.3390/ijms22115608.

[46] S. Barua, S. Mitragotri, Challenges associated with penetration of nanoparticles across cell and tissue barriers: a review of current status and future prospects, Nano Today 9 (2014) 223–243, https://doi.org/10.1016/j.nantod.2014.04.008.

[47] A. Aghamali, M. Khosravi, H. Hamishehkar, N. Modirshahla, M.A. Behnajady, Synthesis and characterization of high efficient photoluminescent sunlight driven photocatalyst of N-Carbon Quantum Dots, J. Lumin. 201 (2018) 265–274, https://doi.org/10.1016/j.jlumin.2018.04.061.

[48] X. Peng, M.C. Schlamp, A.V. Kadavanich, A.P. Alivisatos, Epitaxial growth of highly luminescent CdSe/CdS core/shell nanocrystals with photostability and electronic accessibility, J. Am. Chem. Soc. 119 (1997) 7019–7029, https://doi.org/10.1021/ja970754m.

[49] R. An, F. Zhang, X. Zou, Y. Tang, M. Liang, I. Oshchapovskyy, Y. Liu, A. Honarfar, Y. Zhong, C. Li, H. Geng, J. Chen, S.E. Canton, T. Pullerits, K. Zheng, Photostability and photodegradation processes in colloidal CsPbI 3 perovskite quantum dots, ACS Appl. Mater. Interfaces 10 (2018) 39222–39227, https://doi.org/10.1021/acsami.8b14480.

[50] F. Pinaud, X. Michalet, L.A. Bentolila, J.M. Tsay, S. Doose, J.J. Li, G. Iyer, S. Weiss, Advances in fluorescence imaging with quantum dot bio-probes, Biomaterials 27 (2006) 1679–1687, https://doi.org/10.1016/j.biomaterials.2005.11.018.